

GCOM-C/SGLI
Leaf Area Index (LAI)/ Fraction of Absorbed
Photosynthetically Active Radiation (FAPAR) product
Algorithm Theoretical Basis Document (ATBD)

1 October, 2021 (v3.000)

Kobayashi, T.^{A)}, Ono, Y.^{B)}, Kobayashi, H.^{C)}, Yang, W.^{B)}

^{A)} University of Tsukuba

^{B)} Chiba University

^{C)} Japan Agency for Marine-Earth Science and Technology

Contents

1. Introduction	2
2. Algorithm description	2
2.1 Theoretical description	2
2.2 LUTs used for LAI/FAPAR retrieval	3
2.3 Base map	4
2.4 LAI/FAPAR retrieval	5
3. Inputs and outputs	7
3.1 Input data	7
3.2 Output data	7
3.3 Information about the QA flag	8
3.3.1 Land cover types assigned by the “base map” [bit 08-10]	9
3.3.2 Assigned quality level [bit 11-12]	11
4. Validation plan	11
5. Known issues	13
References	13

1. Introduction

This document is an Algorithm Theoretical Basis Document (ATBD) describing the algorithm of GCOM-C LAI/FAPAR product (Algorithm ID: T2B).

Leaf Area Index (LAI) is defined as one half of the total green leaf area per unit ground surface area. GCOM-C LAI is estimated separately for overstory and understory vegetation because LAI of overstory vegetation and understory vegetation differs in seasonal variation and ecosystem function. The unit of the LAI is m^2/m^2 .

The Fraction of Absorbed Photosynthetically Active Radiation (FAPAR) is defined as the proportion of solar radiation effectively absorbed by green leaves in the photosynthetically active wavelengths (the spectral region from 400 to 700 nm). GCOM-C FAPAR corresponds to white-sky FAPAR, or FAPAR by diffuse radiation by green vegetation.

2. Algorithm description

2.1 Theoretical description

The methodology for retrieving LAI and FAPAR is based on the work by Ono et al [1]. LAI and FAPAR are estimated based on the Look-Up Tables (LUTs) that show the relationship between the SGLI multi-angle atmospherically-corrected surface reflectance data and the LAI or FAPAR [1]. The LUTs are created using a radiative transfer simulator, the Forest Light Environmental Simulator (FLiES) [2], and are fit to the field-observed reference data collected from literatures. The FLiES simulates radiative transfers in the forests and grasslands based on the Monte Carlo ray tracing method. LAI and FAPAR are estimated by the multi-angle SGLI data to optimize the LUTs. Figure 1 shows the processing flow.

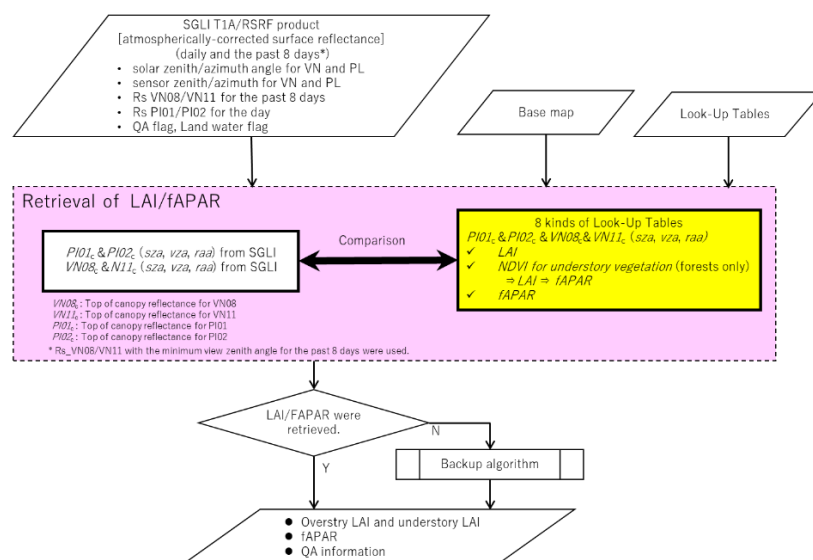


Figure 1. Processing flow

2.2 LUTs used for LAI/FAPAR retrieval

Eight kinds of LUTs are created using FLiES. Each LUT is created from a virtual forest landscape scenarios and input parameters (Figure 2). The virtual forest landscape scenarios consist of the total number of trees, the geometric shapes of the trees, the positions of the trees, and the heights of the trees. They are generated by an empirical forest structure model [9]. The input parameters include the reflectance and transmittance of canopy leaves, the reflectance and transmittance of understory vegetation, the reflectance of stems, and the reflectance of soil (Table 1). They are collected from literatures [3-8]. Virtual forest landscape scenarios in Figure 2 (A), (B), (C), (D), (E) and (F) correspond to dense needle-leaved forest, open needle-leaved forest, dense broadleaved forest, open broadleaved forest, sparse forest, and non-forest areas, respectively. Two types of input parameters are used for the virtual forest landscape scenarios in Figure 2 (C), which corresponds to tropical forests and other broadleaf forests. Two types of input parameters are used for the virtual forest landscape scenarios in Figure 2 (F), which corresponds to paddy fields and grasslands/croplands.

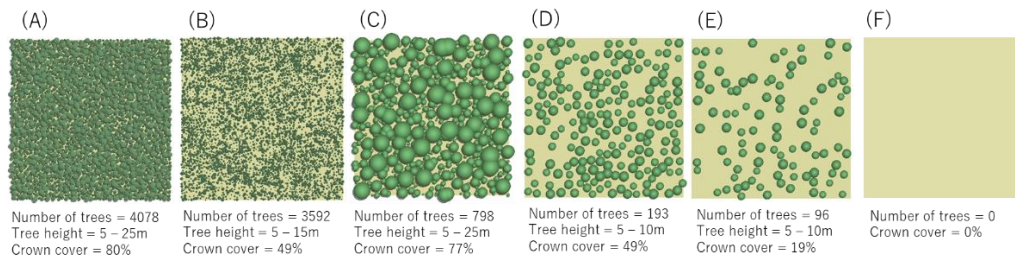


Figure 2. Virtual forest landscape scenarios created for LAI/FAPAR estimation. Two types of input parameters are used for (C) and (F).

Table 1 Parameters used for generating LUTs for LAI/FAPAR retrieval.

Virtual landscape scenarios in Fig.2	Reflectance of leaves (VN08/VN11)	Transmittance of leaves (VN08/VN11)	Reflectance of stem (VN08/VN11)
B	0.0496/0.4024	0.0256/0.4525	0.2220/0.4682
A	0.0494/0.4509	0.0295/0.4101	0.2220/0.4682
D	0.0607/0.4609	0.0368/0.4830	0.2220/0.4682
C	0.0464/0.4545	0.0324/0.5146	0.2220/0.4682
F	0.0881/0.4801	0.0615/0.4958	0.0/0.0
F	0.1043/0.4636	0.0513/0.5024	0.0/0.0
C	0.0571/0.5352	0.0195/0.3914	0.2220/0.4682
E	0.0607/0.4609	0.0368/0.4830	0.2220/0.4682

Multi-angle SGLI data need to match the bidirectional reflectance factor at the top of canopy simulated by FLiES using input parameters and virtual forest landscape scenarios. The input parameters and forest landscape scenarios are selected so that the bidirectional reflectance factor at the top of the canopy can match the multi-angle SGLI data. Consistency between them is checked at several sites where field-observed reference LAI data are available. The field-observed reference LAI data are collected from literatures. LUTs are created for each solar and sensor geometry. Figure 3 shows the flow of LUT creation.

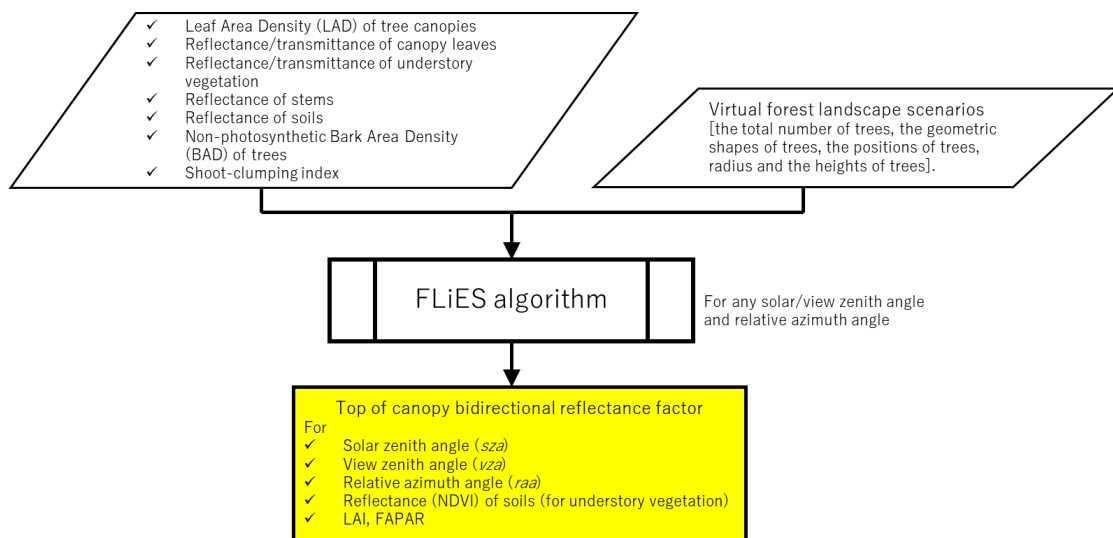


Figure 3. Flow of LUT creation

2.3 Base map

The “base map” has 16 land cover categories: broadleaf evergreen forest, sparse broadleaf forest, very-open broadleaf forest, open broadleaf forest, closed broadleaf forest, sparse or very-open needle-leaf forest, open needle-leaf forest, closed needle-leaf forest, very-closed needle-leaf forest, open mixed forest, closed mixed forest, sparse unknown forest, very-open unknown forest, unknown forest, non-forests and unknown land covers. It was produced using SGLI surface reflectance data and the Global PALSAR-2/PALSAR Forest/Non-Forest maps (https://www.eorc.jaxa.jp/ALOS/palsar_fnf/fnf_jindex20140116.htm). We used the Global PALSAR-2/PALSAR Forest/Non-Forest maps, because croplands and paddy fields with no tree cover could be classified as sparse forest or open forest when only SGLI data was used for classification. Nine different virtual landscape scenarios were

used for mapping: 4 types (very dense, dense, open and very open) of needle-leaf forest, 4 types of broadleaf forest, and non-forest (2 types of leaves). Figure 4 shows the “base map” used in this project.

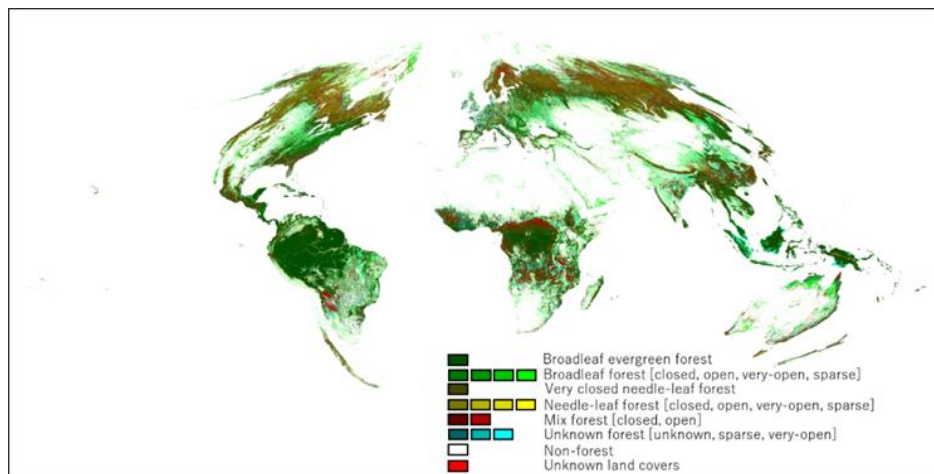


Figure 4. “Base map” used for producing SGLI LAI/FAPAR product. It was produced using SGLI surface reflectance data.

2.4 LAI/FAPAR retrieval

In the GCOM-C product, LAI and FAPAR of the overstory and understory vegetation are estimated from SGLI data using the LUTs (Figure 5). In forest areas, the LAI and FAPAR of the overstory vegetation and the Normalized Difference Vegetation Index (NDVI) of the understory vegetation are retrieved from the LUTs created from the virtual forest landscape scenarios in Figure 2(A)-(E). In non-forest areas, the LAI and FAPAR of understory vegetation are retrieved from the LUT created from the virtual forest landscape scenarios in Figure 2(F), as 0.0 for the LAI and FAPAR of the overstory vegetation. NDVI of understory vegetation (understory NDVI) is later converted into LAI and FAPAR. LAI and FAPAR for water and snow/ice areas are assigned as “no data”.

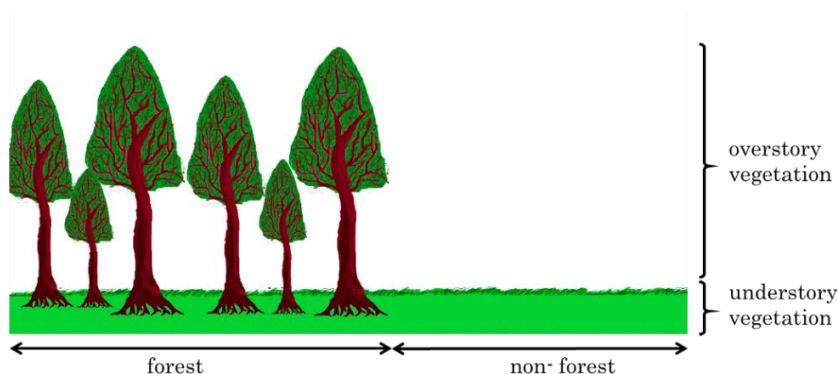


Figure 5. Definition of overstory vegetation and understory vegetation in the GCOM-C LAI/FAPAR product.

A) Retrieved LAI and FAPAR for 1st version

The following value is retrieved as LAI and FAPAR.

- ✧ LAI: Overstory LAI (LAI for overstory vegetation) for forests assigned by “Base map”, and Total LAI (LAI for overstory and understory vegetation) for non-forests assigned by “Base map”. Forests and non-forests do not mean the true land cover types, but the land cover types assigned by “Base map”. For example, overstory LAI is estimated for the grasslands when the land cover type was assigned as forests by “Base map”.
- ✧ Understory NDVI: NDVI of understory vegetation for forests assigned by “Base map”. Understory NDVI is assigned as “0” for non-forests.
- ✧ FAPAR: FAPAR of whole green vegetation (overstory and understory vegetation are included).

B) Retrieved LAI and FAPAR for 2nd version and 3rd version.

The following values are retrieved as LAI.

- ✧ LAI: Total LAI (LAI for overstory and understory vegetation).
- ✧ Overstory LAI: Overstory LAI (LAI for overstory vegetation).
- ✧ FAPAR: FAPAR for whole green vegetation (FAPAR for overstory and understory vegetation).
- ※ “LAI for understory vegetation” = “LAI” – “Overstory LAI”.
- ※ “LAI for forest” in the 1st version = “Overstory LAI” in the 2nd or 3rd version.
- ※ “LAI for grassland” in the 1st version = “LAI” in the 2nd or 3rd version.

In non- forest areas, “Total LAI”, “Overstory LAI” (= 0.0) and “FAPAR” can be retrieved directly using LUTs. In forest areas, “Overstory LAI” can be retrieved directly using LUTs. “Total LAI” and “FAPAR” of forest areas are calculated from “Overstory LAI” and “Understory NDVI” which is also retrieved directly using LUTs. They are calculated as follows.

Total LAI (for forest areas)

“Understory NDVI” is converted into apparent understory LAI by the following equation,

$$LAI_u = 6.7913 * NDVI_u^4 - 4.2145 * NDVI_u^3 - 0.1439 * NDVI_u^2 + 2.2167 * NDVI_u - 0.324 \quad (1)$$
$$(LAI_u = 0.0, \text{ if } NDVI_u < 0.152),$$

where LAI_u is the apparent LAI for understory vegetation, and $NDVI_u$ is the NDVI for understory vegetation. The equation was obtained by fixing the soil type, the vegetation type and sun-target-sensor geometry. Total LAI for forest areas is calculated by adding LAI_u to the LAI of overstory vegetation.

FAPAR (for forest areas)

FAPAR for forest areas are estimated by the equation,

$$FAPAR_t = FAPAR_o + (1 - FAPAR_o - RED_{refl}) * FAPAR_0 \quad (2)$$

$$FAPAR_0 = -0.0071 * LAI_u^4 + 0.0795 * LAI_u^3 - 0.3515 * LAI_u^2 + 0.8125 * LAI_u + 0.0105 \quad (3)$$

where $FAPAR_t$ is the FAPAR for overstory and understory vegetation, $FAPAR_o$ is the FAPAR for overstory vegetation, $FAPAR_0$ is the FAPAR for understory vegetation when there is no overstory vegetation, and RED_{refl} is the reflectance of overstory vegetation for red region. $FAPAR_t$ is the output FAPAR value. The equation is obtained by assuming that the reflection by overstory vegetation is approximately equal to RED_{refl} by fixing the soil type, the vegetation type and sun-target-sensor geometry.

The LUTs used for the LAI/FAPAR estimation are assigned by “base map”. The LUTs used for each land cover category of the “base map” are shown in Table 2.

Table 2 Land cover categories and used LUTs

Code	Land cover classes in the base map	Used LUTs
LC1	Broadleaf evergreen forest	D, E
LC2	Closed broadleaf forest	A, B, C, D
LC3	Open broadleaf forest	D
LC4	Very-open broadleaf forest	D
LC5	Sparse broadleaf forest	D, G, H
LC6	Very-closed needle-leaf forest	A, B
LC7	Closed needle-leaf forest	A, B
LC8	Open needle-leaf forest	B
LC9	Very-open or sparse needle-leaf forest	B, G, H
LC10	Closed mixed forest	A, C
LC11	Open mixed forest	B, D
LC12	Unknown forest	B, D, F, G, H
LC13	Very-open unknown forest	B, D
LC14	Sparse unknown forest	B, D, G, H
LC15	Non-forest areas	G, H
LC16	Unknown land covers	A, B, C, D, G, H

- A) LUT of dense needle-leaved forest (used virtual forest landscape scenarios: A in Figure 2)
- B) LUT of open needle-leaved forest (used virtual forest landscape scenarios: B in Figure 2)
- C) LUT of dense broadleaved forest (used virtual forest landscape scenarios: C in Figure 2)
- D) LUT of open broadleaved forest (used virtual forest landscape scenarios: D in Figure 2)
- E) LUT of tropical forest (used virtual forest landscape scenarios: C in Figure 2)
- F) LUT of sparse forest (used virtual forest landscape scenarios: E in Figure 2)
- G) LUT of paddy fields (used virtual forest landscape scenarios: F in Figure 2)
- H) LUT of grasslands/croplands (used virtual forest landscape scenarios: F in Figure 2)

3. Inputs and outputs

3.1 Input data

The SGLI atmospherically collected land surface reflectance (RSRF) data and geometry data (solar zenith angle, solar azimuth angle, satellite zenith angle and satellite azimuth angle) are used as inputs. The reflectance for nadir direction (VN08 and VN11) and the reflectance for slant direction (PI01 and PI02) are used for the LAI/FAPAR retrieval in forests, while only NDVI is used in non-forests and sparse forests because of the strong influence of soils. SGLI data for the past 7 days are not used in ver. 3, because cloud conditions have a greater influence on LAI/FAPAR retrieval than observation angles. Only NDVI is used for retrieval as a backup algorithm. LAI and FAPAR cannot be retrieved if “no data” or “cloud” is set in the QA flag of RSRF data, or if the land water flag is set to 0 (water).

3.2 Output data

The global SGLI LAI/FAPAR product is supplied as 36×18 Sinusoidal tiles, though 219 tiles are not supplied because they have no valid input data. LAI/FAPAR is estimated for land pixels of each tile (Figure 6). Four layers are provided for daily LAI/FAPAR product (GC1SG1_yyyymmddD01D_Thhvv_L2SG_LAI_Q_3000.h5).

A) For the 1st version: LAI, Understory_NDVI, FAPAR, QA_flag

B) For the 2nd and 3rd version: LAI, Overstory_LAI, FAPAR, QA_flag

Each tile includes approximately 250 m pixels of 4800×4800 . Datatype of each layer are 16-bit unsigned integer. Sample images of the daily global LAI and FAPAR on August 1, 2020 and their composite images from August 1 to August 10, 2020, are shown in Figure 7. A sample image for one-tile can be viewed on the site of “Standard Products and Algorithm”.

(https://suzaku.eorc.jaxa.jp/GCOM_C/data/product_std_j.html)

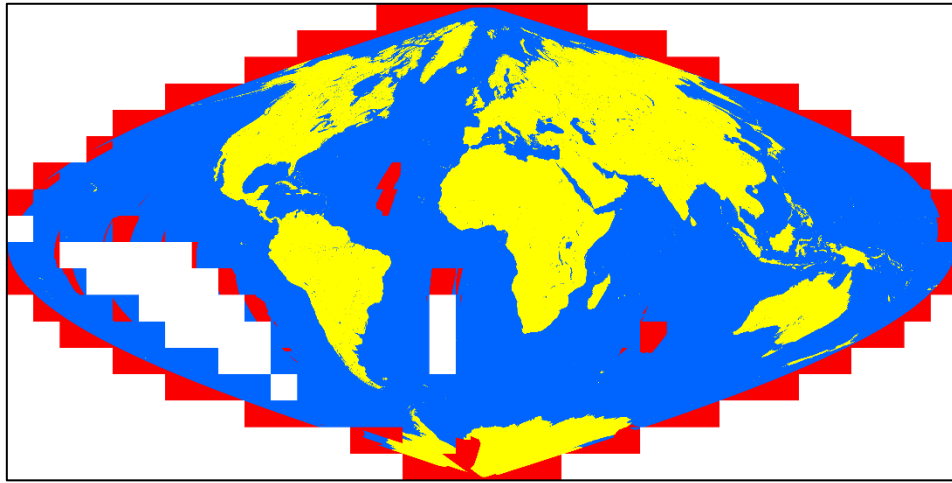


Figure 6. Pixels where LAI/FAPAR is estimated. This figure was created using the 2 months of SGLI data for July and August, 2021. LAI and FAPAR are estimated at yellow-colored pixels. Blue and red pixels are water pixels and pixels with no valid data, respectively. White-colored tiles are tiles with no input data.

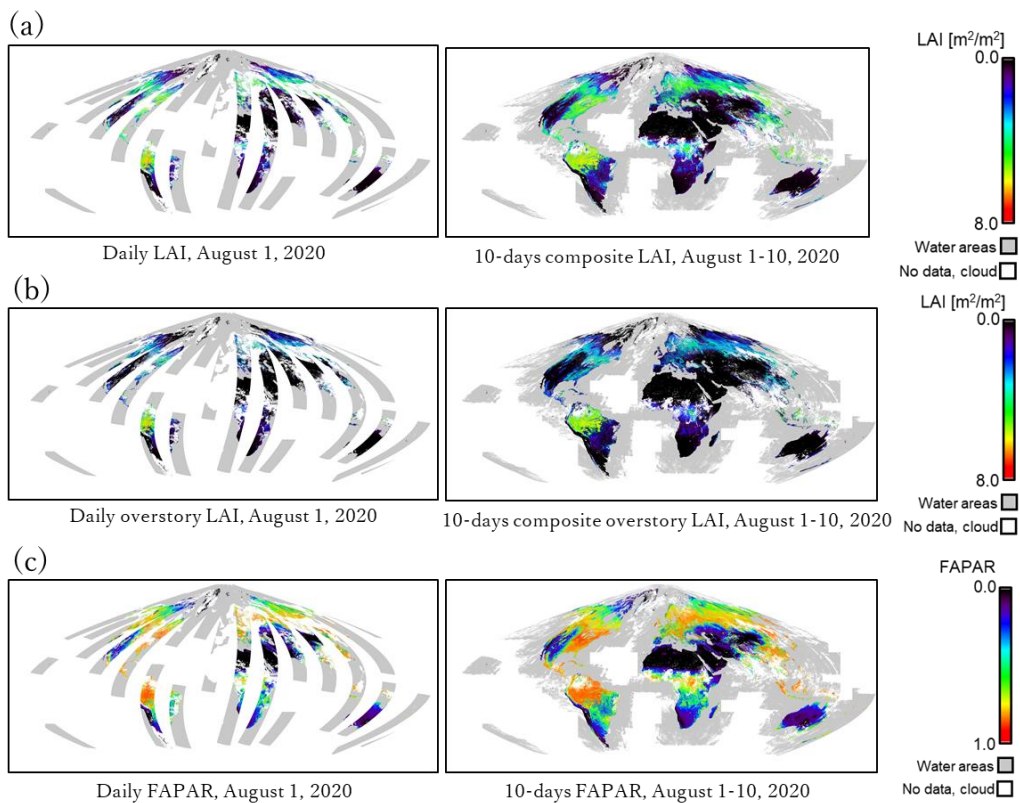


Figure 7. Global maps of LAI (a), Overstory LAI (b) and FAPAR (c). Daily maps are generated using RSRF data for August 1, 2020 as input. Composite maps are generated using daily maps from August 1 to Augusts 10, 2020.

3.3 Information about the QA flag

The explanation of QA_flag is shown in Table 3. It is suggested not to use data with the “cloud shadow”, “quality level: poor or unreliable” or “backup algorithm” bit standing. Data with “bad air condition” bit standing is also of low quality, although there are cases where the bit may be standing at high mountain and certain land covers.

Table 3 Bit specification of QA flag

Bit	Description	Meaning	Level-3 mask
0	no data	Any of input SGLI data has error value	
1	land/water	0: water > 50% of the pixel 1: land > 50% of the pixel	
2	mixed with land/water	0: pure land or pure water 1: The pixel is mixed with land and water	
3	cloud	1: The pixel was assigned as cloud	
4	bad air condition	1: The air condition is not good	
5	snow or ice	1: The pixel was assigned as snow or ice	
6	cloud shadow	1: The pixel was assigned as cloud shadow	mask
7	The condition of sensor zenith angle is not good	0: good 1: sensor zenith angle for nadir direction > 40° or sensor zenith angle for slant direction < 40°	mask
8-10	land cover type	The land cover type assigned by “Base map”	
11-12	quality level	00: good quality 10: acceptable 01: unreliable 11: poor	
13	Value could not be retrieved	1: LAI/FAPAR could not be retrieved	
14	pol cloud or high-tau	1: The pixel was assigned as pol cloud or high-tau	
15	backup algorithm	1: Backup algorithm was applied for the retrieval	mask

3.3.1 Land cover types assigned by the “base map” [bit 08-10]

Bits 08 to 10 correspond to the landcover type assigned in the “base map”. The LUT used for LAI/FAPAR retrieval can be known for each pixel from the information described in 2.4 and these bits.

For the 1st version

A) [bit 08-10: 000]

✓ LC1, LC4

B) [bit 08-10: 100]

✓ LC3

- C) [bit 08-10: 010]
 - ✓ LC2, LC5, LC17
- D) [bit 08-10: 110]
 - ✓ LC6, LC7
- E) [bit 08-10: 001]
 - ✓ LC11
- F) [bit 08-10: 101]
 - ✓ LC12, LC24
- G) [bit 08-10: 011]
 - ✓ LC8, LC9, LC10, LC13, LC14, LC15, LC16
- H) [bit 08-10: 111]
 - ✓ LC18, LC19, LC20, LC21, LC22, LC23

For the 2nd version

- A) [bit 08-10: 000]
 - ✓ LC1, LC2
- B) [bit 08-10: 100]
 - ✓ LC3, LC4
- C) [bit 08-10: 010]
 - ✓ LC5
- D) [bit 08-10: 110]
 - ✓ LC6, LC7
- E) [bit 08-10: 001]
 - ✓ LC11
- F) [bit 08-10: 101]
 - ✓ LC8, LC9, LC10
- G) [bit 08-10: 011]
 - ✓ LC12, LC13, LC14, LC15, LC16, LC17, LC18, LC24
- H) [bit 08-10: 111]
 - ✓ LC19, LC20, LC21, LC22, LC23

For the 3rd version

- I) [bit 08-10: 000]
 - ✓ LC8
- J) [bit 08-10: 100]
 - ✓ LC6, LC7

- K) [bit 08-10: 010]
 - ✓ LC3, LC11
- L) [bit 08-10: 110]
 - ✓ LC2, LC10
- M) [bit 08-10: 001]
 - ✓ LC1
- N) [bit 08-10: 101]
 - ✓ LC4, LC5, LC9, LC12, LC13, LC14
- O) [bit 08-10: 011]
 - ✓ LC15
- P) [bit 08-10: 111]
 - ✓ LC16

3.3.2 Assigned quality level [bit 11-12]

Bits 11 to 12 show the quality of retrieved LAI/FAPAR.

- A) [bit 11-12: 00]

LAI/FAPAR were reasonably retrieved.
- B) [bit 11-12: 10]

LAI/FAPAR were retrieved, though they were retrieved from the insufficient number of values or the variance was high.
- C) [bit 11-12: 01]

LAI/FAPAR were retrieved from the input SGLI data that is of low quality.
- D) [bit 11-12: 11]

LAI/FAPAR were retrieved from much lower quality SGLI data.

4. Validation plan

The accuracy of the retrieved LAI/FAPAR is assessed using the in-situ observation data which are collected at 13 sites around the global. The validation is held mainly on grasslands and forests. Data collected from available databases are also used for validation. Tentative comparison results between ground measured LAI and FAPAR and SGLI retrievals at a pixel level are shown in Figure 8. The ground measured data were mainly contributed by GCOM-C PIs, AKITSU Tomoko, HONDA Yoshiaki, KAJIWARA Koji, KOBAYASHI Hideki, MORIYAMA Masao, NAGAI Shin, NASAHARA Kenlo Nishida, and SUSAKI Junichi ^[13-16].

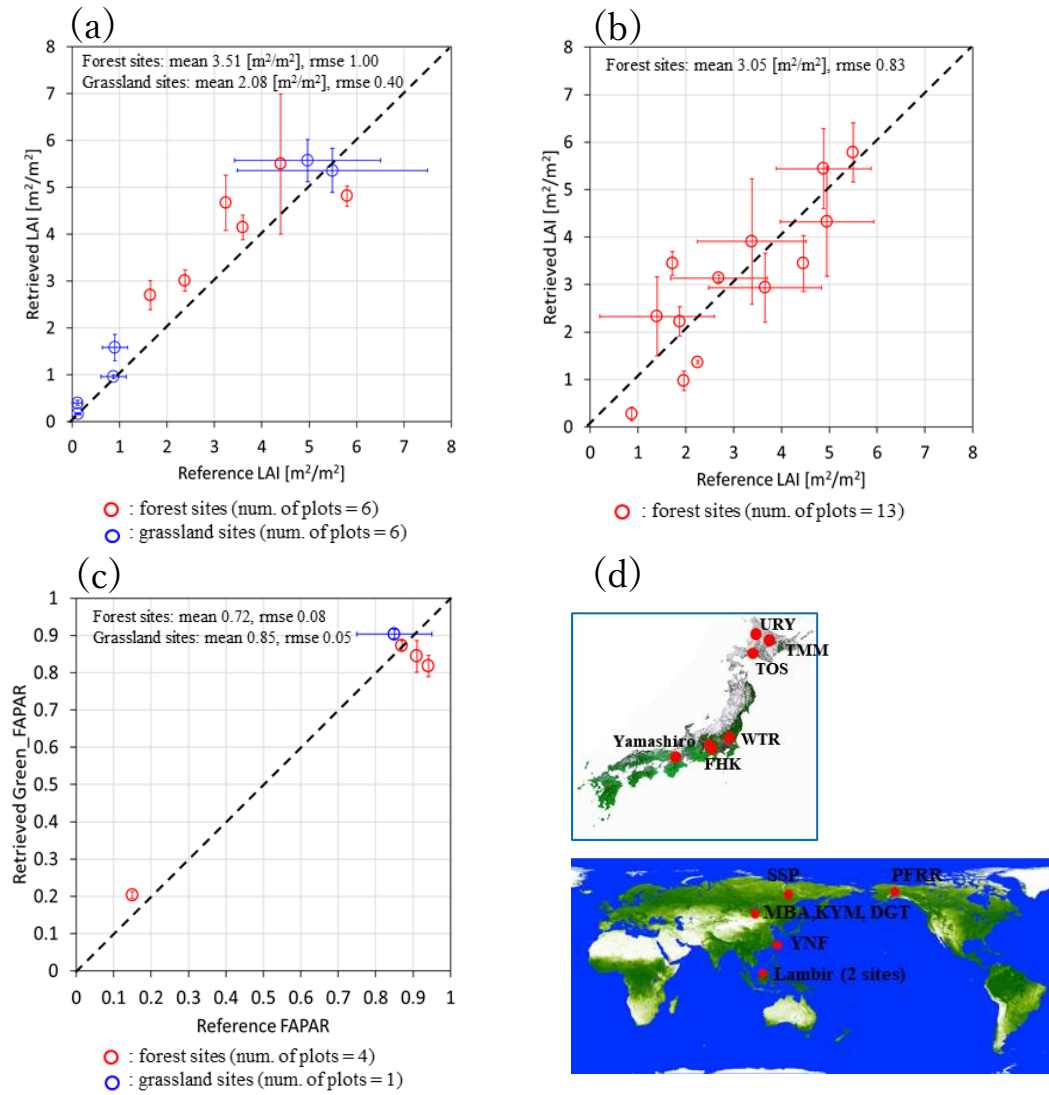


Figure 8. Comparisons between measured LAI and FAPAR, and SGLI retrievals: (a) total LAI, (b) overstory LAI and (c) FAPAR. The reference FAPAR for forest sites in (c) is the total FAPAR, though the retrieved FAPAR is the green FAPAR, which does not include PAR absorption by non-green elements. The distribution of the sites where the measured data were collected is shown in (d): FHK, Fuji Hokuroku Flux Observation site, Japan; Lambir, Lambir Hills site, Malaysia; Lambir Oil Palm, Lambir Oil Palm Plantation site, Malaysia; PFRR, Poker Flat Research Range site, USA; SSP, Spasskaya Pad site, Russia; TMM, Tokachi Mitsumata JAXA Super Site 500, Japan; TOS, Hokkaido University Tomakomai Experimental Forest site, Japan; URY, Hokkaido University Uryu Experimental Forest site, Japan; YNF, Yona Field, Japan; Yamashiro, Yamashiro site, Japan; DGT, Delgertsogt JAXA Super Site 500, Mongolia; KYM, Khar Yamaat JAXA Super Site 500, Mongolia; MBN, Baganuul JAXA Super Site 500, Mongolia; and WTR, Watarase JAXA Super Site 500, Japan.

5. Known issues

- The product has the tendency of overestimating LAI at the open needle-leaved forests.
- Sometimes “Overstory LAI” does not become “0.0” at croplands or grasslands with dense vegetation.
- The accuracy of “LAI” is low at the snow-covered areas.
- “LAI” may be incorrectly estimated in places where the land cover is incorrectly assigned on the “base map”.

References

- [1] Ono, Y., Murakami, H., Kobayashi, H., Nasahara, K., Kajiwara, K. and Honda, Y., 2015. Development of a leaf area index estimation algorithm for GCOM-C/SGLI multi-spectral and multi-angle observation data, the 30th International Symposium on Space Technology and Science, Kobe, Japan, 2015-n-59p.
- [2] Kobayashi, H. and Iwabuchi, H., 2008. A coupled 1-D atmosphere and 3-D canopy radiative transfer model for canopy reflectance, light environment, and photosynthesis simulation in a heterogeneous landscape, *Remote. Sens. Environ*, **112**, pp. 173-185.
- [3] Noda, H. M., Motohka, T., Murakami, K., Muraoka, H., Nasahara, K.H, 2014. Reflectance and transmittance spectra of leaves and shoots of 22 vascular plant species and reflectance spectra of trunks and branches of 12 tree species in Japan, *Ecological Research*, **29**, pp. 111.
- [4] Hosgood, B., Jacquemoud, S., Andreoli, G, Verdebout, J., *et al*, 1995. Leaf Optical Properties EXperiment 93 (LOPEX 93). European Commission: Ispra, Italy.
- [5] Hosgood, B., Jacquemoud, S., Andreoli, G, Verdebout, J., *et al*, 1993. Leaf Optical Properties EXperiment Database (LOPEX 93). Dataset. Available on-line from the Ecological Spectral Information System (EcoSIS): <http://ecosis.org>
- [6] Wu, J., Kobayashi, H., Stark, S. C., Meng, R., Guan, K., *et al*, 2018. Biological processes dominate seasonality of remotely sensed canopy greenness in Amazon evergreen forest, *New Phytologist*, **217**, pp. 1507-1520.
- [7] Meerdink, S. K., Hook, S. J., Roberts, D. A., Abbott, E. A., 2019. The ECOSTRESS spectral library version 1.0. *Remote Sensing of Environment*, **230**, pp. 1–8.
- [8] Baldrige, A. M., Hook, S. J., Grove, C. I., Rivera, G., 2009. The ASTER Spectral Library Version 2.0. *Remote Sensing of Environment*, **113**, pp. 711-715.
- [9] Yang, W., Kobayashi, H., Chen, X., Nasahara, K. N., Suzuki, R., *et al*, 2018. Modeling three-dimensional forest structures to drive canopy radiative transfer simulations of

- bidirectional reflectance factor, *International Journal of Digital Earth*, **11**, pp. 981-1000.
- [10] Arino, O., Bicheron, P., Achard, F., Latham, J., *et al.*, 2008. GLOBCOVER: The Most Detailed Portrait of Earth, *European Space Agency Bulletin*, **136**, pp. 24–31.
<https://earth.esa.int/web/guest/-/globcover-the-most-detailed-portrait-of-earth-5910>.
- [11] ESA (European Space Agency) and UCL (Université Catholique de Louvain), 2011. GLOBCOVER 2009 (Global Land Cover Map). Dataset. Available on-line from
http://due.esrin.esa.int/page_globcover.php
- [12] Tateishi, R., Hoan, N.T., Kobayashi, T., Alsaaidh, B., Tana, *et al.*, 2014. Production of global land cover data – GLCNMO2008, *Journal of Geography and Geology*, **6**, pp. 99-122.
- [13] Akitsu, T. K., Nakaji, T., Yoshida, T., Sakai, R., Mamiya, W., Terigele, Takagi, K., Honda, Y., Kajiwara K., Nasahara, K. N., 2020. Field data for satellite validation and forest structure modeling in a pure and sparse forest of *Picea glehnii* in northern Hokkaido, *Ecological Research*, **2020**, pp.1–15. doi:10.1111/1440-1703.12114.
- [14] Akitsu, T. K., Nakaji, T., Kobayashi, H., Okano, T., Honda, Y., Bayarsaikhan, U., Terigele, Hayashi, M., Hiura, T., Ide, R., Igarashi, S., Kajiwara, K., Kumikawa, S., Matsuoka, Y., Nakano, Ta., Nakano, To., Okuda, A., Sato, T., Tachiiri, K., Takahashi, Y., Uchida, J., Nasahara, K. N., (in press). Large-scale ecological field data for satellite validation in deciduous forests and grasslands, *Ecological Research*, **2020**, doi:10.1111/1440-1703.12155.
- [15] Kobayashi, H., Nagai, S., Kim, Y., Yang, W., Ikeda, K., Ikawa, H., Nagano, H. and Suzuki, R., 2018. In situ observations reveal how spectral reflectance responds to growing season phenology of an open evergreen forest in Alaska, *Remote Sensing*, **10**(7), p.1071. (Data are available from Arctic Data archive System (ADS), Japan, <https://ads.nipr.ac.jp/dataset/A20181212-002>)
- [16] Nagai, S., Kotani, A., Sato, T., Sugimoto, A., Maximov, T. C., Nogovitsyn, A., Miyamoto, Y., Kobayashi, H., and Tei, S., 2020. Direct measurement of leaf area index in a deciduous needle-leaf forest, eastern Siberia, *Polar Science*, **25**(7), doi: 10.1016/j.polar.2020.100550